Giant Polymerlike Micelles Formed by Nucleoside-Functionalized Lipids

Francesca Baldelli Bombelli,[†] Debora Berti,[†] Uwe Keiderling,[‡] and Piero Baglioni*[,†]

Department of Chemistry and CSGI, University of Florence, via della Lastruccia 3, Sesto Fiorentino, 50019 Florence, Italy, and Hahn Meitner Institut, Berlin and TU Darmstadt, Germany

Received: February 19, 2002; In Final Form: July 22, 2002

We report an investigation on the aggregation of 1,2-dilauroyl-sn-glycero-3-phosphatidyluridine (DLPU), a surfactant molecule that merges the self-assembling properties of lecithins with the molecular recognition characteristics of nucleic bases in a phosphate-buffered aqueous solution at physiological pH and as a function of lipid concentration. Because spontaneous self-assembly and interfacial properties are the result of a delicate balance between hydrophobic interactions and polar-head interactions, a structural characterization is essential for a complete and full understanding of base−base properties in the aggregates, as observed by spectroscopic techniques. Small-angle neutron scattering, static light scattering, and quasi-elastic light scattering have been employed to assess the structural evolution of the binary system as the lipid concentration is increased. The data indicate the presence of rather flexible elongated aggregates, whose local structure is cylindrical and remains essentially unchanged during micellar growth. Scattering data are fully supported by cryo-TEM analysis. The results are consistent with micellar unidimensional growth to giant wormlike aggregates that eventually entangle to form a transient network with a response to mechanical stress that is similar to that of polymer solutions in the semidilute range. Such aggregates are known as polymerlike micelles to stress the similarity with the behavior of macromolecules in good solvents. In our case, the correspondence is not limited to a mesosocopic structural scale because from a chemical point of view each monomer contains a nucleic acid functionality that is also expressed in the polymerlike aggregates whose biopolymeric counterpart is in fact a polynucleotide. Therefore, these new aggregates can be considered to be the first example of an "associative polynucleotide".

Introduction

Phosphatidylnucleosides are synthetic surfactant molecules that merge the self-assembling properties of lecithins with the molecular recognition characteristics of nucleic bases.

Such derivatives have a number of possible applications because nucleoside analogues are currently the drug of choice in some antileukemic therapies and in the treatment of the HIV infection.[1,2] The spontaneous self-assembling of phospholiponucleosides into hierarchical structures can be exploited in the delivery step, thus preventing the usually severe toxicity side effects[3] that normally follow the common administration routes of such drugs.

Nucleotides are the constituting monomers of nucleic acids. From a chemical point of view, one DNA strand is a "random" copolymer formed by four different nucleotides. Each strand is coupled through H-bonding to a "complementary" one, that is, to another copolymer that contains a complementary base sequence. Base selectivity, which allows the storage and transmission of chemical information necessary to protein synthesis and to cell life, is connected to the capability of bases to form an H-bonded adduct with the complementary base that is preferred over the other possible combinations. This selectivity is achieved thanks to macromolecular organization, where stacking interaction between neighboring bases plays a major role. Molecular recognition of bases in nucleic acids is a cooperative process.

Starting from this biochemical background, we are interested in the expression of molecular functions in self-organized systems, where the driving force of aggregation has a hydrophobic nature, which is the exclusion of hydrocarbon chains from contact with the aqueous medium. This effect is de facto cooperative, and various topologies such as globular, rigid, or flexible cylindrical micelles or bilayers can be formed as a result of packing preferences of the constituent surfactant molecules. The molecular information (i.e., packing parameter) is then amplified in the supramolecular arrangement and dictates the phase behavior. In this respect, phospholiponucleosides do not represent an exception because the self-assembly can be fine-tuned by a proper choice of the alkyl chains of the lecithin in the synthetic step. Aside from the biological relevance of the nucleosides, most important is the molecular information contained in the polar head. Nucleic acid functionalities are triggered by the macromolecular organization; in our case, it is the self-aggregation that makes base−base interactions possible.

It is well-known that the spontaneous curvature of the surfactant film, determined by its chemical nature and by the condition of the dispersing medium, induces different self-assembled morphologies.[4] We have previously reported some investigations of the "long chain" derivatives 1,2-dioleoyl-sn-glycero-3-phosphatidyluridine and 1,2-dioleoyl-sn-glycero-3-phosphatidyladenosine that prefer locally flat topologies (zero curvature) and also of some "short chain" derivatives, such as 1,2-dioctanoyl-sn-glycero-3-phosphatidylnucleosides, that form quasi-spherical micelles.[5−9] In both cases, it has been possible to show that DNA bases anchored in the hydrophilic corona can interact with each other through a combination of hydrogen

* Corresponding author. E-mail: baglioni@csgi.unifi.it.
[†] University of Florence.
[‡] Hahn Meitner Institut.

10.1021/jp020463m CCC: $22.00
Published on Web 10/16/2002

bonding and base stacking in a way that resemble the Watson−Crick base-pairing recognition. Molecular recognition is then taking place, and it is expressed in a complex structure thanks to self-aggregation.

The spontaneous curvature of the surfactant film can be altered by a so-called "control parameter" such as temperature for nonionic surfactants,[10] ionic strength of the aqueous medium for self-assembled aggregates of ionic surfactants,[11] and cosurfactant concentration.[12]

Aqueous micelles can undergo unidirectional growth with increasing surfactant concentration or salt concentration.[11,13−15] Monodimensional growth is energetically driven by the free energy term $\Delta E = -2E_{\text{end caps}}$, that is, the energy gain to pass from two smaller cylindrical aggregates with four hemispherical end caps to a single cylindrical structure. When this term is favorable, micelles can become very long aggregates characterized by a certain degree of flexibility, depending on their surface charge density, eventually resembling polymer molecules. Above a surfactant crossover concentration c^*, these wormlike micelles can overlap to form a transient network with static and dynamic properties comparable to those of semidilute polymer solutions

There are two major differences between polymer solutions and wormlike micellar systems. The self-assembling nature of the threadlike aggregates implies a growth of the average molecular weight with increasing surfactant volume fraction ϕ and salt content[11] and, according to a mean-field approach,[16] a broad size distribution. In fact,

$$\bar{L} \propto \phi^{1/2} \tag{1}$$

and

$$N(L) \approx \exp\left(-\frac{L}{\bar{L}}\right) \tag{2}$$

where $\bar{L}$ is the weight-averaged chain length and $N(L)$ is the number of chains of length L.

The second difference is due to the transient nature of the network because wormlike micelles break and recombine on a time scale that is dependent on the system and on the chemical conditions.[17]

Static and dynamic light-scattering experiments provide a convenient method to probe the crossover between dilute and semidilute regimes in wormlike micellar solutions. In fact, it has been observed by several authors[18,19] that a maximum in the intensity of the scattered light for a given scattering vector corresponds to the threshold concentration. In the semidilute regime, the properties of the system depend only on the correlation length ξ, which can be visualized as the mesh size of the transient network of overlapping cylindrical micelles.

The properties of the network can be probed by measurements of the static intensity of the scattered light I_S and by determining the cooperative diffusion coefficient D_c, both of which are associated with collective modes of the network. In the semidilute regime, these parameters are independent of the overall length of the micelles and of the micellar kinetics.

Photon correlation spectroscopy yields for polymer solutions a time autocorrelation function of the scattered field that is generally multimodal in the semidilute range.[20] In the short-time domain, one observes a fast mode that depends linearly on the squared wavevector, a typical fingerprint of Brownian diffusive modes. For long time scales, a q-independent mode generally shows up, revealing a second process for which diffusion is not the rate-limiting step.

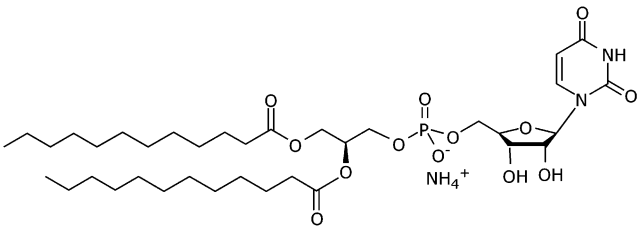

Figure 1. Schematic drawing of the chemical structure of DLPU.

TABLE 1: DLPU Molar Concentrations and Corresponding Volume Fractions in 0.1 M Phosphate Buffer, pH = 7.5

sample	c [M]	ϕ
1	1.0×10^{-3}	5.9×10^{-4}
2	2.0×10^{-3}	1.2×10^{-3}
3	4.0×10^{-3}	2.3×10^{-3}
4	7.5×10^{-3}	4.4×10^{-3}
5	1.0×10^{-2}	5.9×10^{-3}
6	2.0×10^{-2}	1.2×10^{-2}
7	3.0×10^{-2}	1.8×10^{-2}
8	3.5×10^{-2}	2.1×10^{-2}
9	5.0×10^{-2}	2.9×10^{-2}
10	1.0×10^{-1}	5.9×10^{-2}

Information on the static properties of polymerlike micelles can also be gained by combining static light scattering and small-angle neutron scattering. Whereas the former technique probes global static properties of the aggregates, in the latter case, the smaller wavelength permits an increase of the structural resolution even down to the length scale of the cross-sectional radius of the micelles, allowing the determination of the local structure of aggregates.

The outline of this paper is the following: First, light and neutron static scattering data are presented, and the discussion is organized to appreciate the increasing structural resolution as the scattering vector increases. Then a dynamic light-scattering (DLS) analysis allows the observation of the different concentration regimes as the lipid volume fraction is increased. The experimental evidence obtained from scattering techniques is then supported by Cryo-Tem observations in direct space.

Experimental Section

Materials. 1,2-Dilauroyl-sn-glycero-3-phosphocholine was purchased from Avanti Polar Lipids (Alabaster, AL), and its purity was checked by TLC. Because no oxidation or lyso products were detectable, the lecithin was used without further purification. Uridine was purchased from Fluka (Switzerland). Phospholipase D from *Streptomyces sp.* AA586 was a generous gift from Asahi Chemical Industry Co., Ltd. (Japan). Deuterium oxide (>99.5%) for SANS measurements, HCl, $CHCl_3$, MeOH, and NH_3 (33%) were purchased from Fluka as were anhydrous $NaH_2PO_4 \gg 99\%$ and $Na_2HPO_4 \gg 99.5\%$.

Synthesis of 1,2-Dilauroyl-sn-glycero-3-phosphatidyluridine. DLPU (Figure 1) was synthesized starting from the corresponding phosphatidylcholine in a two-phase system[21] according to the method proposed by Shuto and co-workers[22,23] and was obtained as an ammonium salt.

Sample Preparation. The lyophilized powder was dissolved in 0.1 M phosphate buffer at pH = 7.5 prepared in water (for SLS and DLS) or in deuterated water (for SANS). The concentration range investigated and the corresponding volume fractions are shown in Table 1. Cryo-TEM was performed on both water and deuterated water. No morphological differences have been detected for the different solvents.

Static and Dynamic Light Scattering. Light-scattering measurements were performed on a Brookhaven Instrument

apparatus equipped with a BI9000AT correlator and a BI200SM goniometer. The signal was detected by an EMI 9863B/350 photomultiplier. The light source is the second harmonic of a diode-pumped Coherent Innova Nd:YAG laser ($\lambda = 532$ nm) that is linearly polarized in the vertical direction. Measurements were performed at 25 °C. Approximately 1 mL of sample solution was transferred into the cylindrical Hellma scattering cell that was then sealed and centrifuged for about 4 h (the most viscous samples required overnight centrifugation) at a centrifugal relative acceleration of 4863*g* to remove dust particles from the scattering volume.

Data Analysis for Static Light Scattering. Static light scattering (SLS) experiments were performed at 60 different angles in the range $20° \leq \theta \leq 150°$, corresponding to a scattering vector range of 5.4×10^{-4} Å$^{-1} < q = 4\pi n/\lambda \sin(\theta/2) < 3 \times 10^{-3}$Å^{-1}, with the refractive index of the scattering medium $n = 1.33$ and a 5320 Å wavelength. Data have been converted into absolute scattering intensities $\Delta R(q)$ (i.e., excess Rayleigh ratios) using toluene as reference standard according to[24]

$$\Delta R(q) = \frac{\langle \Delta I(q) \rangle}{\langle I_{\mathrm{ref}}(q) \rangle} R_{\mathrm{ref}}(q) \left(\frac{n}{n_{\mathrm{ref}}} \right)^2 \tag{3}$$

where $\Delta\langle I(q)\rangle$ and $\langle I_{\mathrm{ref}}(q)\rangle$ are the excess scattering intensity of the solution and the scattering intensity of the reference solvent toluene, respectively, $R_{\mathrm{ref}}(q) = 2.77 \times 10^{-5}$ cm^{-1} is the Rayleigh ratio of toluene at 5320 Å,[25] and n and n_{ref} are the refractive indexes of the solution and the reference solvent, respectively.

Assuming a scattering law of the form

$$\frac{Kc}{\Delta R(q)} = \frac{1}{M_{\mathrm{app}}}[1 + q^2 \xi_{\mathrm{s}}^{\,2}] \tag{4}$$

a plot of $Kc/\Delta R(q)$ versus q^2 yields the apparent molar mass M_{app} and the static correlation length ξ_{s}. In eq 4, c is the surfactant concentration and $K = 4\pi^2 n^2 (\mathrm{d}n/\mathrm{d}c)^2/(N_{\mathrm{A}}\lambda_0^4)$ is constant for a given wavelength, where $(\mathrm{d}n/\mathrm{d}c)$ is the refractive index increment. The refractive index increment is 1.61×10^{-1} mL/g, as determined by differential refractometry using an RF-600 differential refractometer from C. N. Wood Mfg. Co., Newton, PA.

For samples in the dilute range, the Lorentzian law was obeyed only in the range of $q\xi_{\mathrm{s}} \ll 1$; therefore, only the low q data have been included in the fit. For samples in the semidilute regime, the angular dependence of the scattered intensity is generally well described by eq 4 over the entire q range.[26]

Data Analysis for Dynamic Light Scattering. In dynamic light scattering (DLS) experiments, the normalized time autocorrelation function $g_2(q, t)$ of the scattered intensity is measured according to

$$g_2(q, t) = \frac{\langle I^*(q, 0) I(q, t) \rangle}{\langle I(q, 0)^2 \rangle} \tag{5}$$

For ergodic systems, this function can be expressed in terms of the field autocorrelation function $g_1(q, t)$ through the Siegert relation:

$$g_2(q, t) = A[1 + \beta^2 g_1(q, t)^2] \tag{6}$$

where A is the baseline and β^2 is the coherence factor that is dependent on the scattering geometry and details of the detection system. When the spectral profile of the scattered light can be described by a multi-Lorentzian curve, then $g_1(q, t)$ can be written as the Laplace transform of the spectrum of relaxation times:

$$g_1(q, t) = \int_0^\infty w(\tau)\, \mathrm{e}^{-t/\tau}\, \mathrm{d}\tau \tag{7}$$

τ is the relaxation time characteristic of the system, and $w(\tau)$ is its weight factor in the relaxation-time distribution.

To obtain a distribution $w(\tau)$ of decay rates, a constrained regularization method, CONTIN, developed by Provencher[27] was used to invert the experimental data. A statistical parameter "probability to reject", P, is calculated for each $w(\tau)$ generated by CONTIN. The preferred solution is usually the one characterized by a P value closest to 0.5.

Small-Angle Neutron Scattering. Small-angle neutron scattering experiments were performed on the spectrometer V4 (BENSC-Hahn Meitner Institut-Berlin). Three different configurations (i.e., sample−detector distances: 1, 4, and 16 m) allowed us to cover a range of wave vectors q ($4\pi/\lambda \sin(\theta/2)$) of 3.8×10^{-3} to 0.3 Å^{-1} with a 6.1 Å neutron wavelength and $\Delta\lambda/\lambda < 10\%$. Samples were contained in a flat Hellma quartz cell of 1-mm path length. Deuterated phosphate buffer (0.1 M at pH = 7.5 in D_2O) was chosen as a solvent in order to enhance the scattering contrast and minimize the incoherent background from hydrogen. Data have been reduced according to the standard BENSC procedure[28] for small-angle isotropic scattering. All experiments have been performed at 25 °C.

Cryo-TEM. Cryo-TEM pictures have been obtained in the laboratory of Professor Mats Almgren in the Department of Physical Chemistry, Uppsala University, Sweden. The preparation of the samples has been performed according to the routine procedure of the laboratory.[29] A small droplet of the solution was placed under controlled conditions on a pretreated Cu grid of about 20-μm thickness, which was covered by a perforated cellulose acetate butyrate film. Excess material was removed by a gentle wiping off with a filter paper. Then the specimen was vitrified by a rapid transfer into liquid ethane close to its freezing temperature. The sample examination was performed with a Zeiss 902 A electron microscope operating at 80 kV at 100 K. Images were recorded at underfocus settings of about 2−3 μm.

Results and Discussion

Static Light Scattering. Figure 2 reports the intensity $I(q)$ of the light scattered by DLPU micellar solutions in 0.1 M phosphate buffer (pH = 7.5) for different lipid concentrations. The molecular weight distribution of polymerlike micelles is ruled by thermal equilibrium and is dependent on the monomer volume fraction. A concentration scan, done in order to monitor micellar growth, has to take into account the possible convolution of intermicellar interactions and size distribution in the scattering pattern.[30] Preliminary information can be inferred from the concentration dependence of the scattered intensity.

The concentration increase causes a rise in the intensity until 7.5×10^{-3}M, reflecting strong micellar growth. A further increase of the surfactant concentration produces a decrease of the scattered intensity. This can be better visualized if we consider the forward scattering intensity as a function of the surfactant volume fraction. The low-q limit ($q \rightarrow 0$) of the excess Rayleigh ratio ΔR_0 versus surfactant concentration (see Figure 3) shows the characteristic bell-shaped behavior that is typical of polymerlike micellar solutions. Whereas the first part of the curve is well explained by the expected micellar growth, as predicted by eq 1, the decreasing wing accounts for the decrease of osmotic compressibility. This corresponds to a situation where

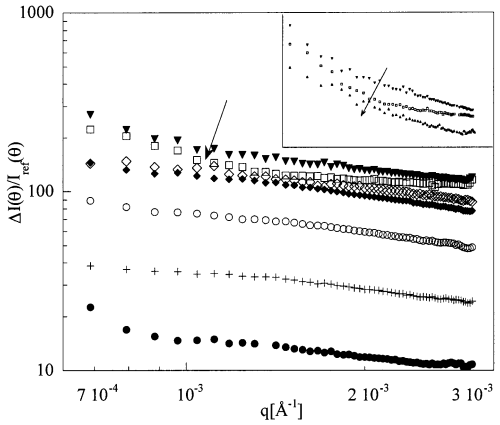

Figure 2. Typical behavior of the normalized scattered intensity $\Delta I(q)/I_{ref}(q)$ versus q for several concentrations of DLPU in 0.1 M phosphate buffer (pH = 7.5) at 25 °C: (●) sample 1, (+) sample 2, (○) sample 3, (◆) sample 4, (◇) sample 5, (▼) sample 6, (□) sample 7. The arrow shows the point where the inversion of the scattered intensity behavior occurs. In the inset, the scattered intensity behavior in the semidilute regime, for samples 6, 7, and 9 is reported.

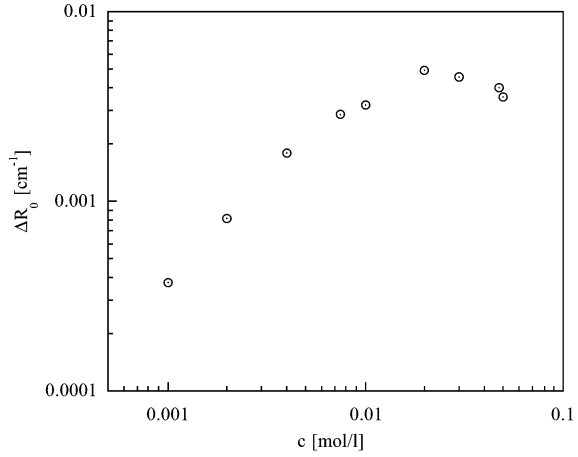

Figure 3. Dependence of the excess Rayleigh ratio ΔR_0 on DLPU concentration in 0.1 M phosphate buffer (pH = 7.5) at 25 °C.

micelles continue growing (a scaling extension of the mean-field theory predicts a power law of $L \propto c^{0.6}$),[31] becoming increasingly entangled to form a micellar network that breaks and recombines according to the micellar scission kinetics.

Above the crossover threshold, the experimental power law ($\Delta R_0 \approx c^{-0.38}$) is in agreement with the scaling exponents reported in the literature[26,32] for micellar networks and predicted by scaling theories for polymers.[33] This finding indicates that the crossover concentration c^* has been exceeded and long threadlike micelles are entangling to form a polymerlike network.[34] A reasonable value that can be estimated from the forward scattering data is around 1×10^{-2}M ($\phi = 0.59\%$).

More quantitative information can be obtained by assuming a Lorentzian scattering law of the form of eq 4 that allows for the determination of the correlation length ξ_S and the apparent molar mass M_{app}.

For $c < c^*$, the law is obeyed in the low-q region, and the correlation length can be related to an effective length of single aggregates, that is, the radius of gyration of the micelles, through $\xi_S = R_g/\sqrt{3}$, with $R_g = \langle R_g^2 \rangle_z^{1/2}$. The apparent molar mass M_{app} is the result of the interplay of the actual micelle size ($\langle M \rangle_w$) with the intermicellar interactions. In the semidilute regime, the scattering law is obeyed over the whole q range, but the

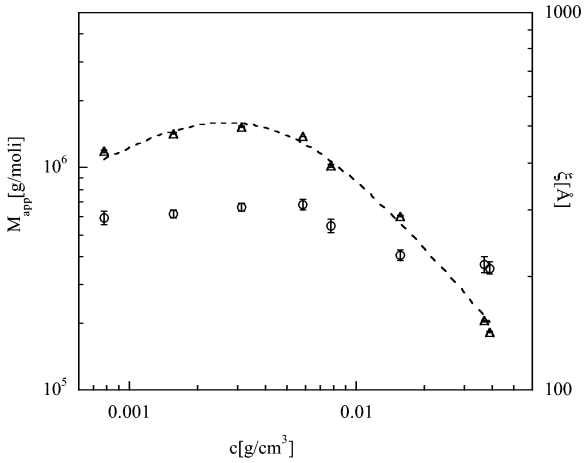

Figure 4. Volume fraction dependence of the static correlation length ξ_S (○) and of the apparent molar mass M_{app} (△) for DLPU in 0.1 M phosphate buffer (pH = 7.5) at 25 °C. The dashed line represents the best fit of the M_{app} data using the expression for the osmotic compressibility of the flexible chains reported in eq 9.

quantities ξ_S and M_{app} have different meanings because light-scattering experiments are now probing the collective features of the transient polymerlike network.[14,26,33] The correlation length can be considered to be a "screening length" for intermicellar interactions in the network and can be visualized as the mesh size of the network. Again, the trend for this quantity as a function of lipid concentration is bell-shaped, as Figure 4 shows, even if the range of concentration tested is not so extended as to appreciate the whole curve shape fully.

Micellar growth is made possible by the relatively high ionic strength provided by the phosphate buffering medium. An analogous concentration scan done in water without added electrolytes yields only very modest micellar growth.[5] Therefore, the screening of electrostatic charges induces a meaningful difference in the chemical potential of a surfactant molecule in the cylindrical body and in the hemispherical cap, and growth along the micellar contour length is favored.

Both M_{app} and ξ_s decrease after 7.5×10^{-3}M, but a comparison between Figures 3 and 4 highlights the fact that the curves are somehow shifted with respect to concentration (i.e., the forward-scattered intensity is still increasing whereas these two quantities already show a decreasing trend). This effect can be explained by considering that the quantity M_{app} is related to the osmotic compressibility $S(0)^{-1}$ according to

$$\Delta R(0) = kCM_{app} = kc\langle M \rangle_w S(0) \tag{8}$$

The complete expression for the osmotic compressibility of flexible polymeric chains has been derived by Ohta and Oono[35] as a function of reduced concentration $X = c/c^*$.

$$S(0)^{-1} = 1 + \frac{1}{8}\left[9x - 2 + \frac{2\ln(1+x)}{x}\right] \times \exp\left[\frac{1}{4}\left(\frac{1}{x} + \left(1 - \frac{1}{x^2}\right)\ln(1+x)\right)\right] \tag{9}$$

The treatment proposed by Schurtenberger et al.[14] to extend this approach to polymerlike micellar solutions has been applied, assuming for $\langle M \rangle_w$ a power law of the form $\langle M \rangle_w = B_1 c^{\alpha}$. The consistent agreement between the experimental data trend and the renormalization group theory is shown in Figure 4, where the continuous line represents the best fit obtained with conventional least-squares techniques.

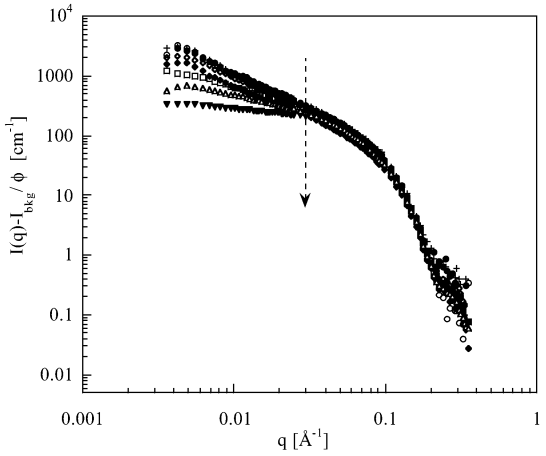

Figure 5. Scattered intensity $I(q)$ versus scattering vector q for semiflexible micelles of DLPU in 0.1 M deuterated phosphate buffer (pH = 7.5) at 25 °C for different concentrations: (●) sample 1, (+) sample 2, (○) sample 3, (◆) sample 4, (◇) sample 5, (□) sample 8, (△) sample 9, (▼) sample 10 (the concentration increases as indicated by the arrow).

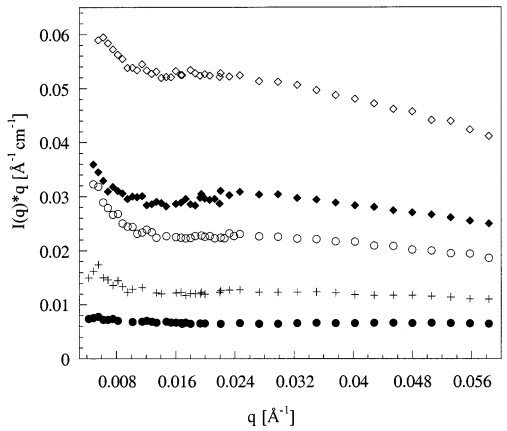

Figure 6. Holtzer or bending-rod plot for polymerlike micelles of DLPU in 0.1 M deuterated phosphate buffer (pH = 7.5) at 25 °C: (●) sample 1, (+) sample 2, (○) sample 3, (◆) sample 4, (◇) sample 5. This representation of SANS spectra emphasizes the region with scaling power −1. In each curve a slope switch is evident highlighting the passage from rigid rods to flexible micelles.

Interestingly, the scaling exponent of micellar molecular weight growth a that is included in the fit as a variation parameter is $0.620 \pm 5 \times 10^{-3}$, in excellent agreement with the predictions of a mean-field approach extended to the semidilute regime.[31] The factor B_1 that appears in the growth power law is also obtainable from the best fit of the same curve is $1.75 \times 10^6 \pm 5\%$ $g^{(1-\alpha)}L^{\alpha}$/mol, confirming consistent micellar growth even for the lowest volume fraction considered.

Small-Angle Neutron Scattering (SANS). The results reported in the previous paragraph agree with the picture of locally cylindrical structures growing along the micellar contour, but decisive evidence is not accessible in that q range. Comprehension of the local structure of polymerlike micelles requires a higher spatial resolution, which can be achieved by small-angle neutron scattering.

The analysis of scattering data from polymerlike micelles can be performed using asymptotic expressions that are valid for the different q regions and provide semiquantitative information. It is important to emphasize that the physical properties on a local scale are not significantly influenced by interaction effects, whereas the situation in the intermediate q range is complicated by the possible presence of a nonnegligible interaggregate structure factor.

Data analysis in the present investigation is performed in a semiquantitative way. It should be mentioned that some authors have recently performed Monte Carlo simulations[37,38] that include a structure factor and polydispersity. Their results present encouraging reliability and account for the invariance of properties such as persistence length. Such kinds of analysis will be reported in a forthcoming paper where we will investigate micelles formed by adenosine, uridine, and their 1:1 mixture derivatives to highlight how the recognition pattern between the complementary bases typical of DNA and RNA affects structural features.[36] Rather than focusing on an analytical approach, this paper focuses on the biological relevance of these supramolecular aggregates that are evidenced for the first time and that we indicate as the first example of living polynucleotides.

Figure 5 shows the small-angle neutron scattering spectra normalized for the volume fraction of micellized DLPU. Spectra show a different pattern in the low q region, indicating a pronounced dependence of the micelle size on the surfactant volume fraction. In the low−intermediate q range, $I(q)$ follows a q^{-1} power law that is typical of the cylindrical structure. The collapse to the same "master" curve in the intermediate−high q region indicates that the local structure is maintained over the whole concentration range investigated. *These observations confirm the presence of long unidimensional aggregates.*

Relevant characteristic length scales for the overall dimension (radius of gyration) and the persistence length (related, for 1D objects, to the bending modulus via the thermal energy k_BT through $l_p = k/k_BT$) are well separated in the reciprocal space.[15]

A very convenient representation for spectra of locally cylindrical objects is the so-called bending rod or Holtzer plot $q^*I(q)$ versus q.[39,40] This plot, shown in Figure 6 for a set of samples at different concentrations, highlights the region with scaling power −1, which is typical of cylindrical structures. A plateau is clearly recognizable for low volume fraction samples as well as a slope change at lower scattering vectors. The slope change is the hallmark of the occurrence of different scaling behavior due to the fact that neutrons are probing different length scales, from rigid rods to flexible chains.

This switch can be correlated to the persistence length of the aggregate in direct space, and some authors have estimated that $q^*l_p \approx 1.9$.[24,41] Such an approach appears inadequate because it does not account for polydispersity effects and for the presence of a structure factor, both of which increase in importance as the concentration is raised. Therefore, the persistence length so calculated is more properly termed the "apparent persistence length" $l_{p,app}$.

From this coarse-grained analysis, we can infer an apparent persistence length that depends linearly on lipid concentration, and this is clearly unphysical, as already observed by several authors;[24] the extrapolation to infinite dilution yields a length of about 120 Å, indicating a rather high flexibility if compared with literature data on polymerlike systems.

We have to regard this number with due caution, and we put off speculation on micellar bending moduli and their dependence on the stacking attitude of the different polar heads to a forthcoming paper based on a Monte Carlo analysis of the SANS data.[36]

However, a simple analysis of the data and qualitative scaling arguments unambiguously demonstrate the flexibility of the aggregates.

In the intermediate−high q region, the cylinder cross section can be determined through a modified Guinier plot, $I(q)^*q$ versus

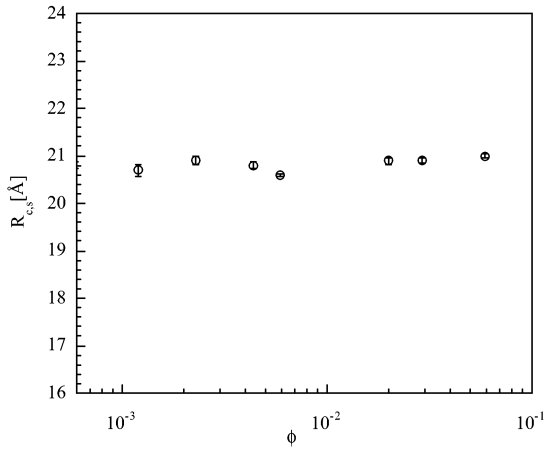

Figure 7. Cross-sectional radius versus volume fraction for DLPU in 0.1 M deuterated phosphate buffer (pH = 7.5) obtained from a modified Guinier plot. The constant value indicates that the local structure is maintained over the whole concentration range.

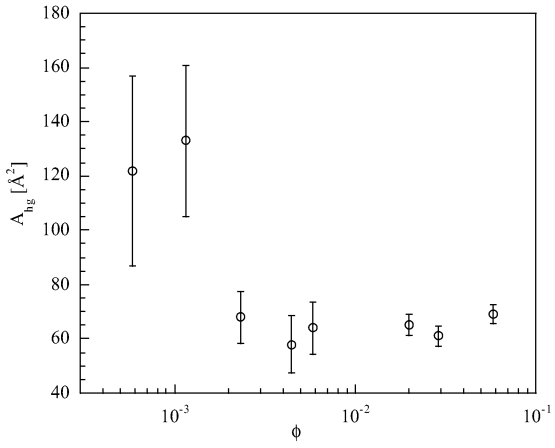

Figure 8. Polar head areas determined by the Porod fitting in the high q region for DLPU in 0.1 M deuterated phosphate buffer (pH = 7.5) at 25 °C.

q^2; following an argument first described by Porod, it is possible to show that this equation is valid:[42]

$$I(q) = \sum_N \frac{C_N}{N} \frac{\pi L_N}{Q} [\int \Delta\bar{\rho}(r)\, \mathrm{d}\bar{A}]^2 * \mathrm{e}^{-q^2 R_c^2/2} \qquad (10)$$

where C_N is the number density of molecules forming an aggregate of N monomers, L_N is the length of the cylinder with aggregation number N, R_c is the radius of gyration of the cross-sectional area of the cylinder (for uniform rodlike particles, $R_c = R/\sqrt{2}$), A is the cross-sectional area, and $\Delta\rho(r)$ is the contrast. Considering A = volume cylinder/L_N, we can write

$$\int \Delta\bar{\rho}(r)\, \mathrm{d}\bar{A} = \frac{1}{L_N} \int \Delta\rho(r)\, \mathrm{d}\nu = \frac{N}{L_N}(b_\mathrm{m} - \rho_\mathrm{S}\nu_\mathrm{m}) \qquad (11)$$

where b_m is the scattering length of the aggregate, ρ_S is the scattering density of the solvent, ν_m is the volume of the aggregate, and N/L_N is independent of micellar size.

After substituting eq 10 into eq 11, we obtain

$$I(q) = (\sum_N c_N) \frac{\pi}{q} \left(\frac{N}{L}\right) (b_\mathrm{m} - \rho_\mathrm{S}\nu_\mathrm{m})^2\, \mathrm{e}^{-R_c^2 q^2/2} \qquad (12)$$

$$\ln(I(q) \cdot q) = \ln\left\{(c - c_\mathrm{cmc})\left(\frac{\pi N}{L}\right)(b_\mathrm{m} - \rho_\mathrm{S}\nu_\mathrm{m})^2\right\} - \frac{R_c^2 q^2}{2} \qquad (13)$$

where $\sum_N c_N = c - c_\mathrm{cmc}$.

The resulting cross-sectional radii plotted as a function of concentration are reported in Figure 7. The radius is around 21 Å and does not depend on lipid concentration. The hydrophobic chain length calculated according to the Tanford model is about 15.4 Å, consistently lower than the cylinder cross section, indicating that SANS are actually monitoring both the phospholiponucleosides hydrophobic chain and the bulky polar headgroup, in agreement with the two-shell model we recently proposed for SANS analysis of globular phospholiponucleoside micelles.[8]

Also connected to the local structure is the weight-averaged aggregation number per unit of length, $\langle N/L \rangle_\mathrm{w}$. This number can be inferred from the intercept of the above-mentioned linear plot, provided that the value of the contrast term $(b_\mathrm{m} - V_\mathrm{m}\rho_\mathrm{s})^2$ is known. Its variance in a narrow range (1.6−1.4 Å^{-1}) demonstrates again the maintenance of the local structure as the surfactant volume fraction is raised.[43]

By moving to higher q values (i.e., increasing the resolution in the direct space), we can determine the surfactants' polar head area at the interface. In this region (the Porod region), the scattered intensity obeys the following asymptotic law:[44]

$$I(q) = 2\pi\left(\frac{S}{V}\right)\Delta\rho^2 q^{-4} + I_\mathrm{bkg} \qquad (14)$$

where S/V is the interface area per volume unit, $\Delta\rho$ is the contrast, and I_bkg is the scattered intensity of the background. By writing

$$\frac{S}{V} = c_\mathrm{s}\Sigma \qquad (15)$$

where c_s is the number density of surfactant molecules and Σ is the polar head area, and knowing the contrast, the polar head areas can be determined from the curve slopes.

The contrast has been evaluated from the Porod invariant, that is, the second moment of the scattered intensity by the system, given by

$$q^* = \int_0^\infty I(q) \cdot q^2 \mathrm{d}q = 2\pi^2(\Delta\rho)^2\phi_1(1 - \phi_1) \qquad (16)$$

where ϕ_1 is the volume fraction of the aggregate. Once subtracted from the experimental intensities, the solvent contribution, and the incoherent background, we can determine the Porod invariant in the following way:[45]

$$q^* = \frac{I(q_\mathrm{min})}{2} \cdot q_\mathrm{min}^3 + \int_{q_\mathrm{min}}^{q_\mathrm{max}} I(q) * q^2\, \mathrm{d}q + \frac{\text{intercept}}{q_\mathrm{max}} \qquad (17)$$

where q_min and q_max are the lowest and highest limits, respectively, of the experimental scattering vectors' range and "intercept" is the intercept of the best linear fit of the Porod limit. A plot of the Porod invariant as a function of $\phi_1(1 - \phi_1)$ yields a straight line[43] with a slope of $2\pi^2\Delta\rho^2$, from which a contrast of 2.6×10^{-11}Å^4 can be obtained, which is in excellent agreement with the contrast obtained from the two-shell model.[8]

Figure 8 shows the resulting polar head areas. Even if the lowest concentration curves are affected by high error, we believe that the discontinuity for 4×10^{-3}M can be connected to a real physical effect that is related to a change in the surfactant aggregation pattern. In fact, at lower concentrations,

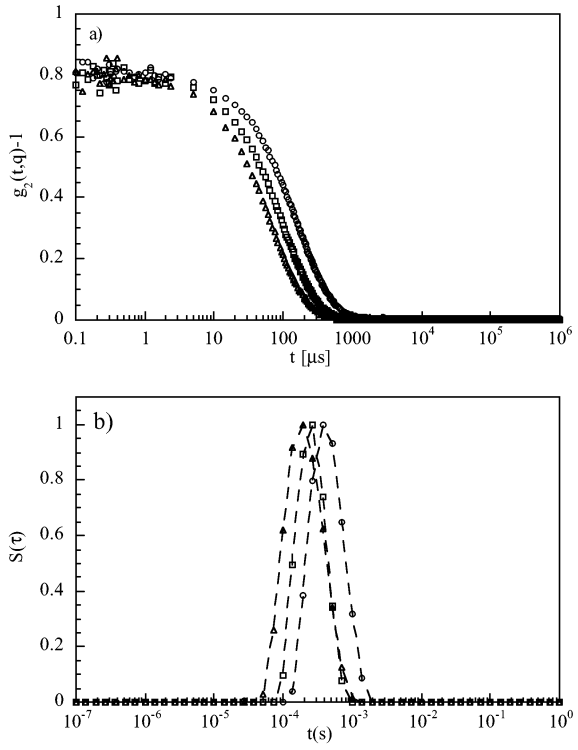

Figure 9. (a) Monomodal autocorrelation functions measured by QELS for sample 2 in the dilute regime at different scattering angles: (○) $\theta = 70°$, (□) $\theta = 90°$, (△) $\theta = 120°$. (b) CONTIN analysis of the autocorrelation functions reported in part a.

the end-cap effects (higher curvature and thus higher polar head areas) are more important, leading to higher values of the areas. When micelles become longer, the contribution of the end caps is more negligible so that the polar head areas level off to an almost constant value. This behavior indicates the presence of long wormlike micelles at about 4×10^{-3} M.

Dynamic Light Scattering. We have performed QELS experiments at 25 °C on samples of DLPU in 0.1 M phosphate buffer in the concentration range 1×10^{-3} to 5×10^{-2}M, exploring both dilute and semidilute regime. The temporal range investigated was 0.1 μs−1 s for samples 1−5 and 1 μs−50 s for samples 6 and 9. DLS measurements have been performed at three different scattering angles for all samples.

The intensity autocorrelation functions are dominated by a single relaxation time (presumably diffusive) until 1×10^{-2}M, the threshold concentration deduced by static light scattering. Figure 9a reports an example of such monomodal autocorrelation functions for sample 2 and for three different scattering vectors (corresponding to 70, 90, and 120° respectively). A Laplace inversion of these autocorrelation functions, performed with the algorithm CONTIN, yields the distributions shown in Figure 9b. The relaxation-time distribution is a single population with some degree of polydispersity; from these data, we obtain the mean relaxation rate $\Gamma(s^{-1})$. If these monomodal autocorrelation functions describe spatial concentration fluctuations, then they decay through a diffusive mechanism, and $g_1(q, t)$ has the exponential form

$$g_1(q, t) \propto \exp(-\Gamma t) \tag{18}$$

where $\Gamma = D_c{*}q^2$.

The collective diffusion coefficient D_c (cm^2/s) is determined from the slope of the curve Γ (s^{-1}) versus q^2 (cm^{-2}). In Figure 10, this linear dependence is reported for samples 1, 2, 3, and

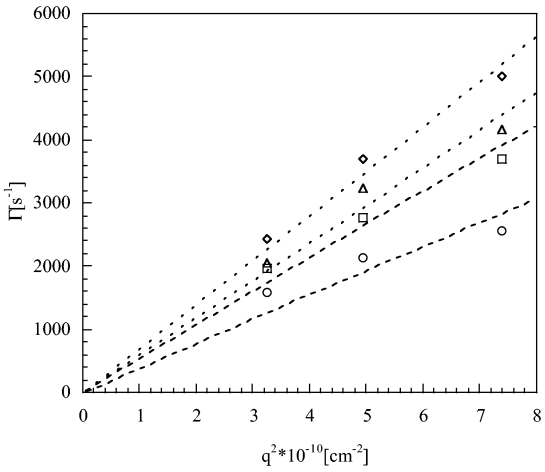

Figure 10. Behavior of G (s^{-1}) versus q^2 (cm^{-2}) for samples in the dilute regime: (◇) sample 1, (△) sample 2, (□) sample 3, (○) sample 5. The collective diffusion coefficient D_c (cm^2/s) is obtained from the slope of these curves. We observe that D_c decreases upon increasing the lipid concentration, reflecting the micellar growth.

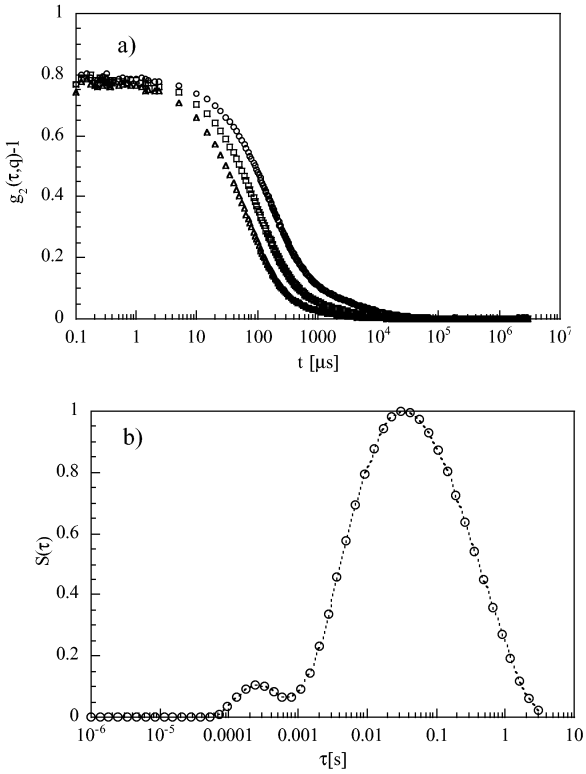

Figure 11. (a) Bimodal autocorrelation functions measured by QELS for sample 6 in the semidilute regime for different scattering angles: (○) $\theta = 70°$, (□) $\theta = 90°$, (△) $\theta = 120°$. (b) CONTIN analysis of the autocorrelation function obtained at 90° reported in part a. We obtain two separated populations, and the slow mode is the dominant relaxation mode.

5; this trend confirms the presence of the diffusive relaxation mechanism. The diffusion coefficients in this regime decrease with increasing concentration, reflecting micellar growth.

Different behavior is found above the threshold concentration, where the autocorrelation functions are bimodal (Figure 11a); CONTIN analysis, reported in Figure 11b for sample 6, shows two well-separated populations. In agreement with some literature on polymers and wormlike micelles,[46] we observe the presence of a "fast" mode and a "slow" mode in the relaxation of the phospholiponucleoside micellar network.

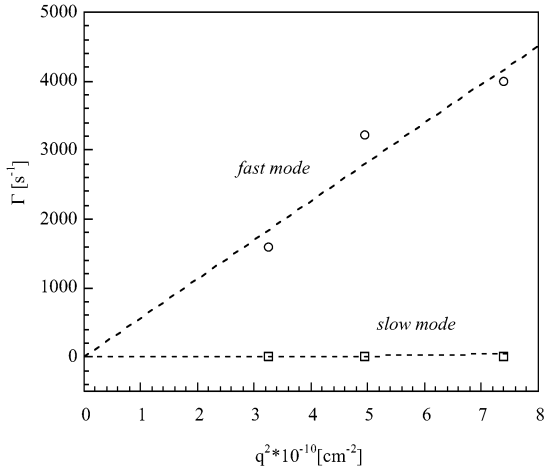

Figure 12. Relaxation rate Γ [s^{-1}] as a function of q^2 [cm^{-2}] for sample 6. One can observe two relaxation modes: the fast mode has a typical diffusive scaling, whereas the slow mode is q-independent.

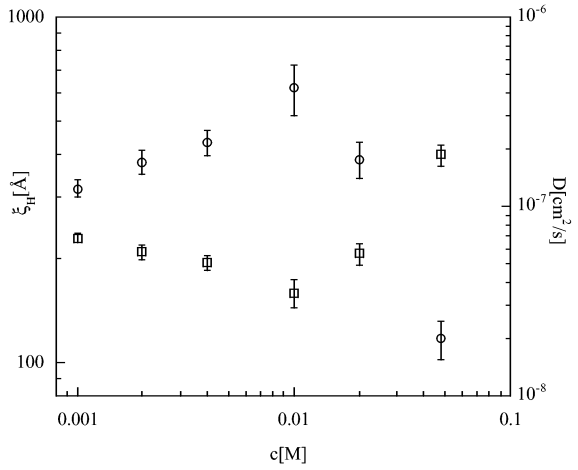

Figure 13. Collective diffusion coefficients D (cm^2/s) (□) and hydrodynamic lengths ξ (Å) (○) as a function of the surfactant concentration. The general behavior reflects the micellar growth in the dilute regime and the formation of a network above the crossover concentration, where the values of ξ_H and D_c reach a maximum and a minimum, respectively.

Candau and co-workers unambiguously showed that the time correlation function of the concentration fluctuations is bimodal for CTAB aqueous micellar solutions in the presence of 0.5 M KBr. In this case, the slow relaxation time results in an invariant q, and it can be related to the global relaxation of the transient network. Moreover, they compared the scaling of the slow relaxation rate with surfactant concentration and temperature to the variation of the terminal time that is determined by means of rheological experiments,[20] concluding a viscoelastic origin of the slow mode.

It is commonly agreed that the fast mode has a diffusive nature, and its rate constant qD_c^2 provides access to the hydrodynamic correlation length ξ_H through the Stokes−Einstein relationship,

$$D_c = k_B T/6\pi\eta_s\xi_H \tag{19}$$

where η_S is the solvent viscosity and k_B is the Boltzmann constant.

On the other side, the real nature of the slow mode and its very occurrence, both in polymeric solutions and in wormlike micellar solutions, are still under debate. For example, Pecora et al.[46−48] have extensively studied nucleic acids by means of PCS and have found two relaxation modes characterized by a diffusive nature even for dilute DNA solutions. Some authors have attributed this slow mode to the dynamics of aggregates or clusters formed by multipolymer chain domains.[49] For the more concentrated DNA solutions, the same authors observed three relaxation modes: a fast mode, a slow mode, and an ultraslow mode that, in this concentration range, represents the main contribution to the dynamics of the solution.

In our case, whereas the fast mode has a typical diffusive scaling, the slow mode results are practically q-independent, as shown in Figure 12. In the pioneering work of Candau, the fast mode represented the main contribution to the relaxation of intensity fluctuations, whereas in our system, as Figure 12b shows, the slow mode is the dominant relaxation mechanism. At present, an exhaustive explanation of this behavior is hampered by the ambiguity present in the literature about the interpretation of the slow mechanism.

We now focus on the concentration dependence of the fast and the slow mode. Figure 13 reports the values of the collective diffusion coefficients obtained by Laplace inversion of the correlation functions; a minimum is present in correspondence of sample 5, formerly (in the static experiments) identified as the "crossover" concentration from the dilute to semidilute regimes. An evaluation of the hydrodynamic lengths through eq 19 yields, as shown in Figure 13, similar behavior to that displayed by the static lengths.

Cryo-TEM. Cryo-TEM allows the direct observation of the presence of flexible polymerlike micelles and of micellar networks. Thus, this technique is ideal to confirm and strengthen the conclusions drawn from scattering techniques. A cryo-TEM analysis has been performed as a function of DLPU volume fraction. Two representative pictures for samples 5 (dilute regime) and 9 (semidilute regime) are reported in Figure 14.

The presence of nonoverlapping threadlike micelles of DLPU is clear for the dilute sample. The aggregates show a rather high flexibility, and some loops are also present. By increasing the surfactant concentration, the threadlike micelles become extremely elongated and form a polymerlike network.

These results confirm the picture that emerged from the combined SANS and light-scattering analysis and demonstrate the formation, for the first time, of polymerlike aggregates where the polar headgroups are formed by "intelligent" nucleosidic units that can perform molecular recognition. These new aggregates can be considered to be the first example of an "associative polynucleotide".

Conclusions

In this paper, we investigated the aggregation properties of 1,2-dilauroyl-sn-glycero-3-phosphatidyluridine (DLPU) in a phosphate-buffered aqueous solution at physiological pH. SANS, static light scattering, and quasi-elastic light scattering show that DLPU form micelles that consistently grow as the lipid concentration is increased and in the presence of added salt, at physiological pH. This behavior is remarkably different from that without added salt. These results indicate the presence of rather flexible aggregates, with a cylindrical structure that remains essentially unchanged during micellar growth. By analogy to polymer solutions, above a surfactant volume fraction threshold, the scattering properties do not follow monotonic behavior, suggesting micellar entanglement. In conclusion, we showed that phospholiponucleoside can form, under appropriate conditions, aggregates that behave like polymer solutions. The main advantage of our system consists of the intelligent polar

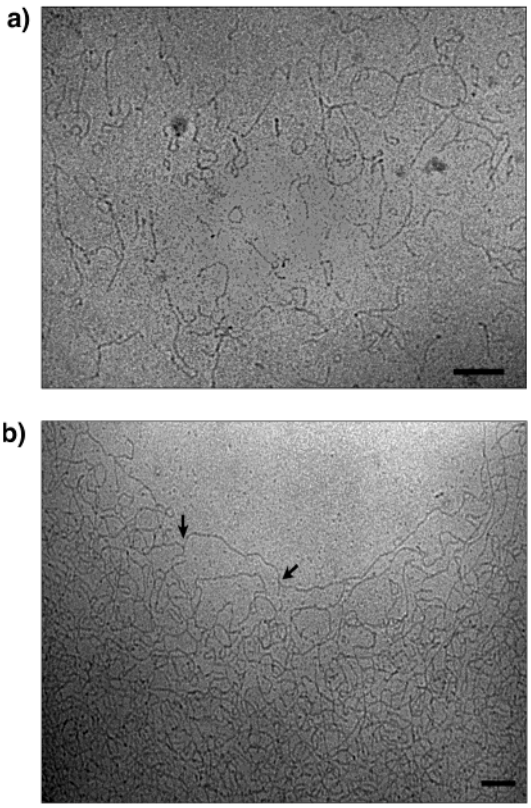

Figure 14. (a) Cryo-TEM image of sample 3 at $T = 25$ °C. The micrograph shows the presence of threadlike micelles not yet overlapped. The micelles appear to be flexible and form some loops. (b) Cryo-TEM image of sample 9 at $T = 25$ °C. The threadlike micelles become very long and form a polymerlike network; the arrows show 3-fold junctions. Bar = 100 nm

headgroup that can reproduce the functionality typical of DNA and RNA and can be considered to be an associative nucleic acid.

We anticipate that the adenosine derivative, where stacking interactions between polar headgroups are present, behaves in different way than the uridine surfactant and then the 1:1 mixture. The formation of a "micellar polynucleotide" opens up new and interesting opportunities in the study of molecular recognition processes of biological interest and in biotechnologies.

Acknowledgment. Financial support from MIUR (PRIN-2001) and CSGI is acknowledged. The experiments at BENSC in Berlin were supported by the European Commission under the Access to Research Infrastructures Action of the Human Potential Program (contract: HPRI-CT-1999-00024). The collaboration of Professor Mats Almgren for the cryo-TEM pictures is thankfully acknowledged. Thanks are due to F.S. Candau for stimulating discussions. We also gratefully acknowledge the detailed and constructive criticism of both referees.

References and Notes

(1) Tedeschi, A.; Montillo, M.; Ferrara, F.; Nosari, A.; Mele, G.; Copia, C.; Leoni, P.; Morra, E. *Eur. J. Haematol.* **2000**, *64*, 182.

(2) Balzarini, J.; Baba, P.; Pauwels, P.; Herdewijn, P.; de Clerq, E. *Biochem. Pharmacol.* **1988**, *37*, 2847

(3) Richman, D. D.; Fischl, M. A.; Grieco, M. H.; Gottileb, M. S.; Volderling, P. A.; Laskin, O. L.; Leedom, J. M.; Groopman, J. E.; Mildvan, D.; Hirsch, M. S.; Jackson, G. G.; Durack, D. T.; Nusinoff-Lehrman, S. N. *N. Engl. J. Med.* **1987**, *317*, 192.

(4) Safran, S. A. In *Structure and Dynamics of Strongly Interacting Colloids and Supramolecular Aggregates in Solution*; Chen, S.-H., Huang, J. S., Tartaglia, P., Eds.; Kluwer Academic: Dordrecht, The Netherlands, 1992.

(5) Berti, D.; Keiderling, U.; Baglioni, P. *Prog. Colloid Polym. Sci.* **2002**, *120*, 64−73.

(6) Berti, D.; Franchi, L.; Baglioni, P.; Luisi P. L. *Langmuir* **1997**, *13*, 3438−3444.

(7) Berti, D.; Bonaccio, S.; Barsacchi-Bo, G.; Luisi, P. L.; Baglioni P. *J. Phys. Chem. B* **1998**, *102*, 303−308.

(8) Berti, D.; Pini, F.; Teixeira, J.; Baglioni P. *J. Phys. Chem. B* **1999**, *103*, 1738−1745.

(9) Berti, D.; Barbaro, P. L.; Bucci, I.; Baglioni P. *J. Phys. Chem. B* **1999**, *103*, 4916−4922.

(10) Olsson, U.; Schurtenberger, P. *Langmuir* **1993**, *9*, 3389.

(11) Cates, M. E.; Candau, S. J. *J. Phys.: Condens. Matter* **1990**, *2*, 6869.

(12) Stradner, A.; Glatter, O.; Schurtenberger, P. *Langmuir* **2000**, *16*, 5354−5364.

(13) Lequeux, F.; Candau, S. J. In *Structure and Flow in Surfactant Solutions;* Prud'homme, R. K., Ed.; ACS Symposium Series 578; American Chemical Society: Washington, DC, 1994; p 51.

(14) Schurtenberger, P.; Cavaco, C.; Tiberg, F.; Regev, O. *Langmuir* **1996**, *12*, 2894−2899.

(15) Magid, L. J. *J. Phys. Chem. B* **1998**, *102*, 4064−4074.

(16) Mukerjee, P. *J. Phys. Chem.* **1972**, *76*, 565.

(17) Cates, M. E. *Macromolecules* **1987**, *20*, 2289.

(18) Candau, S. J.; Hirsch, E.; Zana, R. *J. Physique* **1984**, *49*, 511.

(19) Candau, S. J.; Hirsch, E.; Zana, R. *J. Colloid Interface Sci*. **1985**, *105*, 521.

(20) Buhler, E.; Munch, J. P.; Candau, S. J. *J. Phys. II* **1995**, *5*, 765−787.

(21) Berti, D. Reactivity and Molecular Recognition in Organized System. Ph.D. Thesis, University of Florence, Florence, Italy, 1996.

(22) Shuto, S.; Ueda, S.; Imamura, S.; Fukukawa, K.; Tsujino, M.; Matsuda, A.; Ueda, T. *Chem. Pharm. Bull*. **1988**, *36*, 209.

(23) Shuto, S.; Ueda, S.; Imamura, S.; Fukukawa, K.; Matsuda, A.; Ueda, T. *Tetrahedron Lett.* **1987**, *28*, 199.

(24) Jerke, G.; Pedersen, J. S.; Egelhaaf, S. U.; Schurtenberger, P. *Langmuir* **1998**, *14*, 6013.

(25) The Rayleigh ratio of toluene at 5320 Å has been evaluated by extrapolation of the data reported in Pike, E. R.; Pomeroy W. R. M.; Vaughan, J. M. *J. Chem. Phys.* **1975**, *62*, 318, taking into account its linear scaling with the fourth power of the wavelength.

(26) Schurtenberger, P. In *Light Scattering Principles and Development*; Brown, W., Ed.; Oxford University Press: Oxford, U.K., 1996; Chapter 9.

(27) Provencher, S. W. *Comput. Phys. Commun.* **1982**, *27*, 213−272,.

(28) Keiderling, U. *BerSANS Data Reduction Manual*, Internal Report, HMI, Berlin, 1994.

(29) Mays, H.; Almgren, M.; Dedinaite, A.; Claesson, P. M. *Langmuir* **1999**, *15*, 8072−8079.

(30) Schurtenberger, P.; Cavaco, C. *Langmuir* **1994**, *10*, 100.

(31) Cates, E. M. *J. Phys. (Paris)* **1988**, *49*, 1593.

(32) Appel, J.; Porte, G. *Europhys. Lett.* **1990**, *12*, 185.

(33) Doi, M.; Edwards, S. F. *The Theory of Polymer Dynamics*; Oxford University Press: Oxford, U.K., 1987.

(34) de Gennes, P. G. *Scaling Concepts in Polymer Physics*; Cornell University Press: Ithaca, NY, 1979.

(35) Ohta, T.; Oono, Y. *Phys. Lett. A* **1982**, *89*, 460.

(36) Baldelli Bombelli, F.; Berti, D.; Pini, F.; Baglioni, P. To be submitted for publication.

(37) Pedersen, J. S.; Laso, M.; Schurtenberger, P. *Phys. Rev. E: Stat. Phys., Plasmas, Fluids, Relat. Interdiscip. Top.* **1996**, *54*, 6.

(38) Pedersen, J. S.; Schurtenberger, P. *Macromolecules* **1996**, *29*, 7602.

(39) Holtzer A. *J. Polym. Sci.* **1955**, *17*, 432.

(40) Denkiger, P.; Burchard, W. *J. Polym. Phys*. **1991**, *29*, 589.

(41) Marignan, J.; Appell, J.; Bassereau, P.; Porte, G.; May, R. P. *J. Phys. (Orsay, Fr.)* **1989**, *50*, 3553−6024.

(42) Lin, T.; Chen, S.; Gabriel, N. E.; Roberts, M. F. *J. Phys. Chem.* **1987**, *91*, 406−413

(43) Baldelli Bombelli, F.; Berti, D.; Keiderling, U.; Baglioni, P. *Appl. Phys. A* **2002**, *75*, 1−4.

(44) Porod, G. In *Small Angle X-ray Scattering*; Glatter, O., Krakty, O., Eds.; Academic Press: London, 1982; Chapter 2, pp 17−51.

(45) Cantú, L.; Corti, M.; Del Favero, E.; Dubois, M.; Zemb, Th. N. *J. Phys. Chem. B* **1998**, *102*, 5737.

(46) Borsali, R.; Nguyen, H.; Pecora, R. *Macromolecules* **1998**, *31*, 1548−1555.

(47) Nicolai, T.; Mandel, M. *Macromolecules* **1989**, *22*, 438.

(48) Newman, J.; Tracy, J.; Pecora, R. *Macromolecules* **1994**, *27*, 6808.

(49) Wissenburg, P.; Odijk, T.; Cirkel, P.; Mandel, M. *Macromolecules* **1995**, *28*, 2315.